Available online at www.sciencedirect.com
SCIENCE DIRECT®
Journal of Chromatography A, 1028 (2004) 105–119
JOURNAL OF CHROMATOGRAPHY A
www.elsevier.com/locate/chroma

Heterogeneity of the surface energy on unused C_{18}-Chromolith adsorbents in reversed-phase liquid chromatography

Fabrice Gritti [a,b], Georges Guiochon [a,b,*]

[a] *Department of Chemistry, University of Tennessee, Knoxville, TN 37996-1600, USA*
[b] *Division of Chemical Sciences, Oak Ridge National Laboratory, Oak Ridge, TN 37831-6120, USA*

Received 21 July 2003; received in revised form 11 November 2003; accepted 19 November 2003

Abstract

Single-component adsorption isotherm data were acquired by frontal analysis (FA) for phenol and caffeine on a new C_{18}-Chromolith column (Merck, Darmstadt, Germany), using a water-rich mobile phase (methanol/water, 15/85, v/v). These data were modeled for best agreement between the experimental data points and the adsorption isotherm model. The adsorption-energy distributions, based on the expectation–maximization (EM) procedure, were also derived and used for the selection of the best isotherm model. The adsorption energy distributions (AEDs) for phenol and caffeine converged toward a trimodal and a quadrimodal distribution, respectively. Energy distributions with more than two modes had not been reported before for the adsorption of these compounds on packed columns. The third high energy mode observed for both phenol and caffeine seems to be specific of the surface of the monolithic column while the first and second low energy modes have the same physical origin as the two modes detected on packed columns. These results suggest significant differences between the structures of the porous silica in these different materials.

Keywords: Isotherm modeling; Column reproducibility; Adsorption isotherms; Frontal analysis; Monolithic columns; Affinity energy distribution; Band profiles; Multi-Langmuir isotherm; Phenol; Caffeine

1. Introduction

Mainly for economical reasons, the modeling of overloaded band profiles in liquid chromatography has recently become a topic of great interest [1–3]. It provides an accurate tool to predict the influence of various experimental parameters on the profiles of chromatographic bands at high concentrations, hence to optimize the recovery yield and production rate of a given separation. It is based on the calculation of numerical solutions of the differential mass balance equation of chromatography and requires the prior knowledge of the thermodynamic and kinetic parameters of the system studied. The thermodynamic parameters are most accurately acquired by frontal analysis (FA) [1,4–6] but other experimental approaches (e.g., elution by characteristic point [1,7,8], pulse methods [1,9,10]) may be used when they accommodate the technical and financial requirements (e.g., the data acquisition time and the chemicals prices). The kinetic parameters are often estimated through an apparent dispersion coefficient or from kinetic parameters derived by parameter identification, according to the choice of model of chromatography (equilibrium dispersive, transport dispersive, or the general rate models [1]). The effect of the kinetics on the position and shape of the band profiles is most often secondary when low molecular mass compounds and high loading factors are involved. It requires only a correction of reasonable accuracy. The essential information is then contained in the adsorption isotherm of the compound between the two phases. The determination of accurate adsorption data becomes the most crucial factor to achieve a satisfactory prediction of the experimental band profiles.

FA is an accurate method of measurement of absolute adsorption data which requires only a low minimum column efficiency. It is based on the mass conservation of the compound studied. However, isotherm determination requires a relatively high density of data points acquired in a wide concentration range. It is strongly recommended to perform the measurements in the widest possible range of concentrations, between the limit of detection and the solubility in the mobile phase, and to acquire at least 20 data points,

* Corresponding author. Tel.: +1-865-974-0733; fax: +1-865-974-2667.
E-mail address: guiochon@utk.edu (G. Guiochon).

0021-9673/$ – see front matter © 2004 Elsevier B.V. All rights reserved.
doi:10.1016/j.chroma.2003.11.089

denser in the concentration range where the isotherm curvature is stronger. In the literature, simple models (e.g., the Langmuir model) are most often used to account for adsorption data. This is acceptable as a first approximation and this provides an estimate of the overall adsorption energy of the system. However, this may hide the existence of high energy sites whose role in the retention mechanism may be important despite a reduced density of these sites on the surface [11,12]. We recently reported that the influence of secondary sites of a C_{18}-Kromasil packed column on the retention of phenol and caffeine increases with increasing water content of an aqueous-organic mobile phase [13]. The adsorption energy distribution (AED) was bimodal, as supported by the results of the expectation–maximization procedure which derive the affinity energy distribution from the raw adsorption data. The physicochemical interpretation of this energy heterogeneity remains open. It can be due to the existence of accessible active sites still present on the bare silica or to the heterogeneity of the layer of C_{18}-bonded chains [12].

In this work, we measured the adsorption data of phenol and caffeine by FA in a phase system made of methanol/water (15:85, v/v) and a C_{18}-bonded monolithic column from Merck that had not been used before. The monolith column was used as received from the manufacturer. It did not suffer any of the possible surface property modifications that might arise from an extensive use of a column with a wide variety of different chromatographic systems. We calculated the affinity energy distribution of these two compounds, validated the choice of the best isotherm model, and investigated the origin of the surface heterogeneity of the stationary phase.

2. Theory

2.1. Determination of Single-component isotherm data by frontal analysis

Frontal analysis is the most accurate chromatographic method used to determine single-component isotherms, [1,4]. It consists in the step-wise replacement of the stream of mobile phase percolating through the column with streams of solutions of the studied compound of increasing concentrations and in the recording of the breakthrough curves at the column outlet. Mass conservation of the solute between the times when the new solution enters the column and when the plateau concentration is reached allows the calculation of the adsorbed amount, q^*, of the solute in the stationary phase at equilibrium at the corresponding mobile phase concentration, C. This amount is best measured by integrating the breakthrough curve (equal area method) [14]. The adsorbed amount q^* is given by:

$$q^* = \frac{C(V_{eq} - V_0)}{V_a} \tag{1}$$

where V_{eq} and V_0 are the elution volume of the equivalent area and the hold-up volume, respectively, and V_a is the volume of stationary phase. This relationship applies to all breakthrough curves recorded. This method was used for the acquisition of all the experimental isotherm data measured on the monolith column.

2.2. Calculation of the adsorption energy distributions

Actual surfaces are neither homogeneous nor paved with homogeneous tiles, as it is generally assumed in chromatography. Actual surfaces are characterized by an adsorption energy distribution that may have several more or less well resolved modes, each mode having a finite width. The experimental isotherm on such a surface is the sum of the isotherms on each one of the types of homogeneous sites covering the surface. Under the condition of a continuous adsorption energy distribution and assuming a Langmuir local isotherm model, the experimental isotherm can be written [15]:

$$q^*(C) = \int_0^\infty F(\epsilon) \frac{b(\epsilon)C}{1 + b(\epsilon)C} \, d\epsilon \tag{2}$$

where $q^*(C)$ is the total amount of solute adsorbed on the surface at equilibrium with a concentration C, ϵ the binding energy between an adsorbed solute molecule and the surface of the adsorbent, and b the associated binding constant related to ϵ through the following equation:

$$b(\epsilon) = b_0 \exp\left(\frac{\epsilon}{RT}\right) \tag{3}$$

where b_0 is a preexponential factor that is usually assumed to be the same, whatever the type of adsorption sites i [15].

The normalization condition for the AED is:

$$\int_0^\infty F(\epsilon) \, d\epsilon = q_s \tag{4}$$

where q_s is the overall saturation capacity.

To characterize the behavior of a heterogeneous surface, the AED, $F(\epsilon)$, is derived from a set of experimental isotherm data (with M experimental data points), a procedure for which there is a variety of methods [15–18]. Most of these methods use a preliminary smoothing of the experimental data, e.g., fit these data to an isotherm model, or search for an AED that is given by a certain function, which is chosen depending on the problem studied. In both types of methods, some arbitrary information is injected into the determination of the AED. In this work, we used instead the EM method [18]. This computer-intensive method uses directly the raw experimental data, without injecting any arbitrary information into the AED derivation. The distribution function, $F(\epsilon)$, is discretized, using an N-grid points in the energy space, (i.e., assuming that the surface is tiled with a set of N different homogeneous surfaces) and the corresponding values of $F(\epsilon)$ are estimated from the experimental data points. The energy space is limited by ϵ_{min}

and ϵ_{max}, two energy boundaries which are respectively related to the maximum and the minimum concentrations within which the adsorption data have been acquired, by using Eq. (3) (with $b_{min} = 1/C_M$, $b_{max} = 1/C_1$). However, a narrower range may be considered, as long as it accommodates the data. The amount $q(C_j)$ of solute adsorbed at concentration C_j is iteratively estimated by:

$$q^k_{cal}(C_j) = \sum_{\epsilon_{min}}^{\epsilon_{max}} F^k(\epsilon_i) \frac{b(\epsilon_i)C_j}{1 + b(\epsilon_i)C_j} \Delta\epsilon$$
$$j \in [1, M];\ i \in [1, N] \quad (5)$$

with

$$\Delta\epsilon = \frac{\epsilon_{max} - \epsilon_{min}}{N - 1} \quad \epsilon_i = \epsilon_{min} + (i - 1)\,\Delta\epsilon \quad (6)$$

The index k indicates the kth iteration of the numerical calculation of the AED function. The initial guess (iteration $k = 0$) of the AED function, $F(\epsilon_i)$, is the uniform distribution (over the N fictitious adsorption sites) of the maximum adsorbed amount that was observed experimentally [18]. Using this initial guess has the advantage of introducing the minimum bias into the AED calculation.

$$F^0(\epsilon_i) = \frac{q(C_M)}{N} \quad \forall i \in [1, N] \quad (7)$$

Actually, the EM program calculates the amount adsorbed by taking $b(\epsilon_i)$ as the variable in the energy space, so that neither the temperature nor the preexponential factor in Eq. (3) need to be defined [18]. Only M, N, b_{min}, b_{max} and the number of iterations must be defined before starting the calculations. It is noteworthy that, to obtain any information on the adsorption energy, an assumption must be made regarding the value of b_0 in Eq. (3). The final result is the distribution of the equilibrium constants (often called the affinity distribution). The distribution function is updated after each iteration by:

$$F^{k+1}(\epsilon_i) = F^k(\epsilon_i) \sum_{C_{min}}^{C_{max}} \frac{b(\epsilon_i)C_j}{1 + b(\epsilon_i)C_j} \Delta\epsilon \frac{q_{exp}(C_j)}{q^k_{cal}(C_j)} \quad (8)$$

The EM procedure protects better than most other methods against the consequences of the possible incorporation of experimental artifacts into the calculation of the AED or against the effect of modeling the experimental data (and particularly the noise and drift that the data may contain) [18].

2.3. From the isotherm data to the isotherm model

The following strategy [19] was followed systematically to determine the isotherm model that best accounts for the raw adsorption data measured by FA. The following "tools" were used in that order:

- First, *the Scatchard data plot* (i.e., the plot of q^*/C versus q^*) was used for a first selection among the possible isotherm models. A library of isotherm models can be classified according to the shape of the experimental Scatchard plot. For instance (see Fig. 1), a linear Scatchard plot with a negative slope is characteristic of the Langmuir model, a decreasing convex upward Scatchard plot is, among others, characteristic of the (homogeneous) Jovanovic isotherm and a decreasing convex downward Scatchard plot is, among others, characteristic of the (heterogeneous) bi-Langmuir isotherm model.

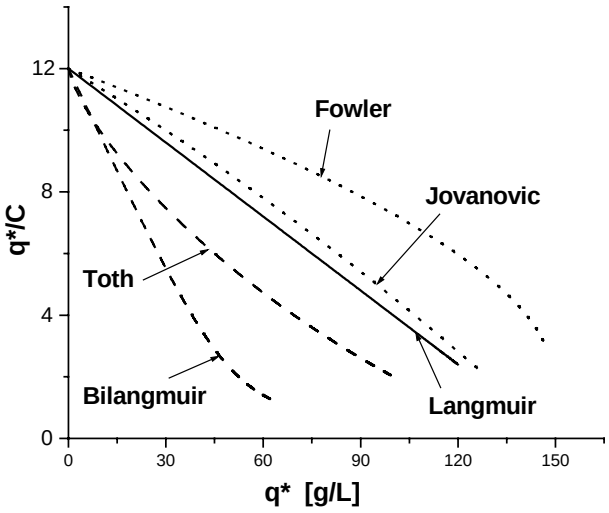

Fig. 1. Correlation between the shape of the Scatchard plot representation (q^*/C vs. q^*) and the nature of the isotherm model.

- Second, *isotherm modeling*: Once the sublibrary of isotherm models consistent with the experimental shape of the Scatchard plot is selected, a nonlinear regression analysis of these models was carried out, using a fitting based on the Marquardt algorithm [20], which minimizes the residual sum of the squares of the relative differences between the experimental data and the model calculations. Then, the statistical Fisher "tool" was used to find out the best isotherm model, after the values of the Fisher parameter, $F_{calc,t}$, calculated for the different models according to:

$$F_{calc,t} = \frac{N - l}{N - 1} \frac{\sum_{i=1}^{i=N} (q_{exp,i} - \overline{q_{exp}})^2}{\sum_{i=1}^{i=N} (q_{exp,i} - q_{t,i})^2} \quad (9)$$

where $q_{exp,i}$ is the experimental values of the solid phase concentrations of the adsorbate in equilibrium with a liquid phase at concentrations C_i, $\overline{q_{exp}}$ the mean value of the data, $q_{exp,i}$, $q_{t,i}$ the estimate given by the model for the solid phase concentration of the adsorbate in equilibrium with the mobile phase concentration C_i, l the number of adjusted parameters in the model, and N the number of experimental data acquired by FA.

Then, between two models $\mathcal{M}_{t_1}$ and $\mathcal{M}_{t_2}$, the F-test ratio F_{t_1,t_2} is calculated by:

$$F_{t_1,t_2} = \frac{F_{calc,t_1}}{F_{calc,t_2}} \quad (10)$$

Considering a risk α, the model $\mathcal{M}_{t_1}$ correlates better the experimental data than the model $\mathcal{M}_{t_2}$ if:

$$F_{t_1,t_2} \geq F_{N-l_1,N-l_2,\alpha} \quad (11)$$

where l_1 and l_2 are the numbers of adjusted parameters in the models $\mathcal{M}_{t_1}$ and $\mathcal{M}_{t_2}$, respectively. $F_{N-l_1,N-l_2,\alpha}$ is available in statistical test tables. If, for a given model $\mathcal{M}_{t_2}$, Eq. (11) is true whatever the model $\mathcal{M}_{t_1}$ then the model $\mathcal{M}_{t_2}$ will be definitively eliminated.

- Third, *affinity energy distribution*: This tool is more sophisticated. It consists in calculating the affinity energy adsorption from the raw adsorption data, as described in the previous section. This allows the selection of the best isotherm model that is consistent with the results of the AED calculations. For instance, if the EM calculations converge toward a bimodal distribution, a Toth model cannot account properly for the isotherm data since the theoretical AED of the Toth model is unimodal.
- Finally, *band profiles*: If after the third row of selection, there are still more than one isotherm model susceptible to account for the adsorption data, the last and final selection is based on the comparison between the calculated and the experimental band profiles at high and low concentrations.

2.4. Modeling of high-concentration, high-performance liquid chromatography

The overloaded band profiles were calculated using the best model of the isotherm of the compound studied and the equilibrium-dispersive model (ED) of chromatography [1,4,21]. The ED model assumes instantaneous equilibrium between the mobile and the stationary phase and a finite column efficiency originating from an apparent axial dispersion coefficient, D_a, that accounts for the dispersive phenomena (molecular and eddy diffusion) and also for the non-equilibrium effects that take place in a chromatographic column. These effects are supposed to be small, otherwise the ED model is not valid. The axial dispersion coefficient is related to the experimental parameters through the following equation:

$$D_a = \frac{uL}{2N} \quad (12)$$

where u is the mobile phase linear velocity, L the column length, and N the number of theoretical plates or apparent efficiency of the column. In the ED model, the mass balance equation for a single component is written:

$$\frac{\partial C}{\partial t} + u\frac{\partial C}{\partial z} + F\frac{\partial q^*}{\partial t} = D_a\frac{\partial^2 C}{\partial z^2} \quad (13)$$

where q^* and C are the stationary and the mobile phase concentrations of the adsorbate, respectively, t the time, z the distance along the column, and $F = (1-\epsilon_t)/\epsilon_t$ the phase ratio, with ϵ_t the total column porosity at time t and distance z. If ϵ_t is assumed to be constant so is F. q^* is related to C through the isotherm equation, $q^* = f(C)$.

2.4.1. Numerical solutions of the ED model

The mass balance equation was integrated numerically using a computer program based on an implementation of the method of orthogonal collocation on finite elements (OCFE) [22–24]. The set of discretized ordinary differential equations was solved with the Adams-Moulton method, implemented in the VODE procedure [25]. The relative and absolute errors of the numerical calculations were 10^{-6} and 10^{-8}, respectively.

2.4.2. Initial and boundary conditions for the ED model

At $t = 0$, the concentration of the solute in the column is uniformly equal to zero, and the stationary phase is in equilibrium with the mobile phase components (methanol and water in this work). The boundary conditions used are the classical Danckwerts-type boundary conditions [1,26] at the inlet and outlet of the column. In all the calculations, the inlet profiles were supposed to be rectangular profiles.

3. Experimental

3.1. Chemicals

The mobile phase used in this work, whether for the determination of the adsorption isotherm data or for the recording of large or small size band profiles, was a mixture of methanol and water (15:85, v/v). Both solvents were HPLC grade, purchased from Fisher Scientific (Fair Lawn, NJ, USA). The mobile phase was filtered before use on a surfactant-free cellulose acetate filter membrane, 0.2 μm pore size (Suwannee, GA, USA). Thiourea was chosen to measure the column hold-up volume at the different methanol contents in the mobile phase. Thiourea, phenol and caffeine were obtained from Aldrich (Milwaukee, WI, USA).

3.2. Materials

The new 100 mm × 4.6 mm Chromolith column (serial UM20622, #30) used was generously offered by Merck (Darmstadt, Germany, EU). These columns are C_{18}-bonded, end-capped, porous silica. The main characteristics of the bare porous silica and of the bonding material used are summarized in Table 1, according to the manufacturer. The total porosity of the monolithic column ($\epsilon_T = 0.867$) was derived from the retention times of two consecutive injections of thiourea after the column was equilibrated during 1 h at the given mobile phase composition.

3.3. Apparatus

The breakthrough curves and the overloaded band profiles of phenol and caffeine were acquired using a Hewlett-Packard (Palo Alto, CA, USA) HP 1090 liquid chromatograph. This instrument includes a multi-solvent delivery

Table 1
Physico-chemical properties of the monolithic silica column supplied by the manufacturers (Merck)

Skeleton size	1.3–1.5 μm
Macropore size	2 μm
Mesopore size	130 Å
Surface area (before C_{18} bonding)	300 $m^2\,g\,l^{-1}$
Surface coverage (C_{18})	3.6 $mmol\,m^{-2}$
Total porosity[a]	0.867
Total carbon	19.5%
Endcapping	Yes

[a] Measured with a methanol/water (15/85, v/v) mixture as the mobile phase.

system (three tanks, volume 1 l each), an auto-sampler with a 250 μl sample loop, a column thermostat, a diode-array UV-detector, and a data station. Compressed nitrogen and helium bottles (National Welders, Charlotte, NC, USA) are connected to the instrument to allow the continuous operations of the pump, the auto-sampler, and the solvent sparging. The extra-column volumes are 0.068 and 0.90 ml, as measured from the auto-sampler and from the pump system, respectively, to the column inlet. All the retention data were corrected for this contribution. The flow-rate accuracy was controlled by pumping the pure mobile phase at 23 °C and 1 ml min^{-1} during 50 min, from each pump head, successively, into a volumetric glass of 50 ml. The relative error was less than 0.4%, so that we can estimate the long-term accuracy of the flow-rate at 4 μl min^{-1} at flow rates around 1 ml min^{-1}. All measurements were carried out at a constant temperature of 23 °C, fixed by the laboratory air-conditioner. The daily variation of the ambient temperature never exceeded ±1 °C.

3.4. Frontal analysis isotherm measurements on the Chromolith column

In order to make accurate measurements of adsorption isotherm data, the retention factor, k' should be neither too high (which limits the number of data points that can be acquired within a reasonable period of time) nor too low (which would cause a decrease in the accuracy of the adsorption data). Values of k' between 2 and 6 are ideal to achieve a precise, accurate isotherm determination. This is the case for these two compounds with a 15/85 (v/v) methanol/water solution as the mobile phase. Then, the retention factor of both phenol and caffeine are between 4 and 6. Prior to any isotherm measurements, the solubilities at 23 °C (the temperature at which the isotherm data were acquired) of the two compounds in the mobile phase were determined approximately by the stepwise addition of 0.5 ml of the pure mobile phase into a volume of 25 ml of a saturated solution containing a small amount of undissolved compound, until complete dissolution. Accordingly, the maximum concentrations used in the FA measurements were 75 and 27 g l^{-1} for phenol and caffeine, respectively. Two master sample solutions were prepared, with concentrations of 10 and 100% of these maximum concentrations, respectively and two consecutive sequences of FA measurements were carried out with these two solutions (see procedure below), giving an accurate isotherm determination at both low and high concentrations. Twenty-six experimental adsorption data points were recorded for each compound.

One pump of the HPLC instrument was used to deliver to the column a stream of the pure mobile phase, the second pump a stream of the pure master sample solution. The concentration of the studied compound in the stream percolating through the column is determined by the concentration of the master sample solution and by the ratio of the flow rates delivered by the two pumps. The breakthrough curves are recorded successively at a flow rate of 1 ml min^{-1}, with a sufficiently long time interval between each breakthrough curve to allow for the reequilibration of the column with the pure mobile phase. The injection time of each new solution were set long enough (typically between 5 and 10 min) to reach a stable plateau at the column outlet. Two overloaded band profiles (one at low column loading, the other at high column loading) needed for the validation of the fitted isotherms were recorded at the time when the frontal analysis experiments were carried out. An isotherm is acceptable only if it accurately predicts the band profiles at both low and high column loadings. To avoid recording any UV-absorbance signal larger than 1500 mAU and the associated too large signal noise, the detection of the breakthrough curves and the overload band profiles of phenol and caffeine were carried out at 291 and 307 nm, respectively. The detector responses for the samples were calibrated accordingly.

4. Results and discussion

4.1. Measurement of the adsorption isotherm of phenol on the Chromolith performance column

Fig. 2A shows the isotherm data of phenol measured by FA at 23 °C, at concentrations from 0 to 75 g l^{-1} in the mobile phase. The isotherm is convex upward as confirmed by Fig. 2B, showing that the Scatchard plot is convex downward. As a result, the Langmuir model, for which the Scatchard plot is linear, cannot account for the adsorption data. The same conclusion can be drawn for the Jovanovic, the Fowler, and the Jovanovic–Freundlich isotherm models, which all generate convex upward Scatchard plots. Accordingly, the number of isotherm models that may describe the adsorption data of phenol is markedly restricted. Among the catalogue of isotherms leading to convex downward Scatchard plots, we list below the simplest ones, by increasing number of model parameters, from a minimum of $l = 3$ to the maximum that allows convergence of the parameters during the fitting procedure ($l = 6$). These models,

described in [15], are:

$l = 3$: The Langmuir–Freundlich (LF) isotherm model

$$q^* = q_s \frac{(bC)^\nu}{1 + (bC)^\nu} \tag{14}$$

The Toth (T) isotherm model

$$q^* = q_s \frac{bC}{[1 + (bC)^\nu]^{1/\nu}} \tag{15}$$

$l = 4$: The bi-Langmuir (L–L) isotherm model

$$q^* = q_{s,1} \frac{b_1 C}{1 + b_1 C} + q_{s,2} \frac{b_2 C}{1 + b_2 C} \tag{16}$$

$l = 5$: The Langmuir/Toth (L–T) isotherm model

$$q^* = q_{s,1} \frac{b_1 C}{1 + b_1 C} + q_{s,2} \frac{b_2 C}{[1 + (b_2 C)^\nu]^{1/\nu}} \tag{17}$$

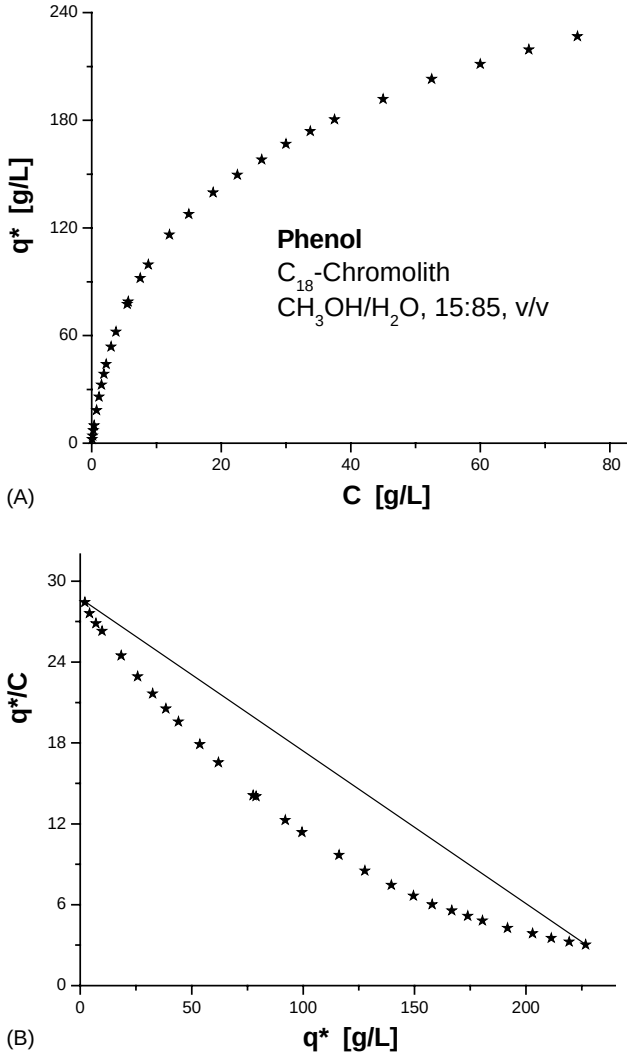

Fig. 2. Experimental isotherm (A) and Scatchard plot (B) of phenol on the Chromolith column #30. Mobile phase methanol/water, 15/85 (v/v). $T = 296\,\mathrm{K}$.

The Langmuir/Langmuir-Freundlich (L–LF) isotherm model

$$q^* = q_{s,1} \frac{b_1 C}{1 + b_1 C} + q_{s,2} \frac{(b_2 C)^\nu}{1 + (b_2 C)^\nu} \tag{18}$$

$l = 6$: The bi-Langmuir–Freundlich (LF–LF) isotherm model

$$q^* = q_{s,1} \frac{(b_1 C)^{\nu_1}}{1 + (b_1 C)^{\nu_1}} + q_{s,2} \frac{(b_2 C)^{\nu_2}}{1 + (b_2 C)^{\nu_2}} \tag{19}$$

The BiToth isotherm (T–T) model

$$q^* = q_{s,1} \frac{b_1 C}{[1 + (b_1 C)^{\nu_1}]^{1/\nu_1}} + q_{s,2} \frac{b_2 C}{[1 + (b_2 C)^{\nu_2}]^{1/\nu_2}} \tag{20}$$

The tri-Langmuir (L–L–L) isotherm model

$$q^* = q_{s,1} \frac{b_1 C}{1 + b_1 C} + q_{s,2} \frac{b_2 C}{1 + b_2 C} + q_{s,3} \frac{b_3 C}{1 + b_3 C} \tag{21}$$

In all these models, $q_{s,i}$, b_i and ν_i stand for the saturation capacity, the adsorption constant, and the heterogeneity factor of site i, respectively. We recall that [15] the distributions of adsorption energy of the Langmuir, Langmuir-Freundlich and Toth isotherm models are a single energy distribution function (a δ-Dirac function), a symmetrical quasi-Gaussian function and a non symmetrical energy distribution with a broadening toward the low energies, respectively. The F_{t_1,t_2} F_{ratio}-test values are tabulated in Table 2. Whatever the pair of models $\{\mathcal{M}_{t_1}; \mathcal{M}_{t_2}\}$ considered, providing a risk α of 1%, $\mathcal{M}_{t_1}$ is statistically better than $\mathcal{M}_{t_2}$ if $F_{t_1,t_2} \geq 2.74$. Accordingly, the isotherm models LF, T and L–L must be eliminated at this stage of the selection. None of the five remaining isotherm models is better than the other four models, at least on the basis of the statistical results of the fitting procedure. The choice

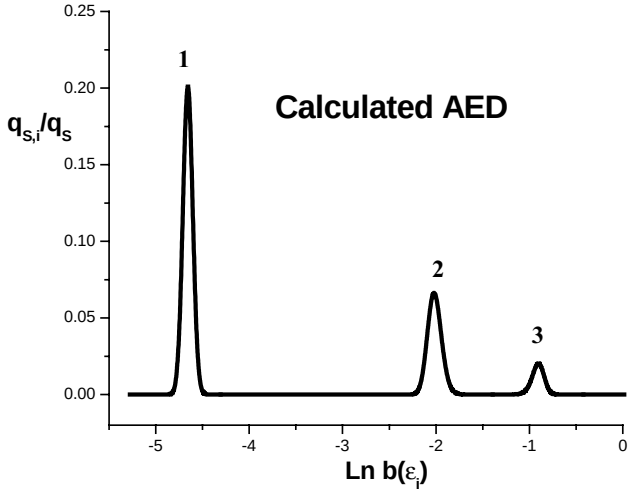

Fig. 3. Affinity energy distribution (AED) of phenol on the Chromolith column, calculated by using the expectation–maximization method (EM). 10^8 iterations required. The AED is plotted as the fraction of the adsorbent surface as a function of the logarithm of the adsorption constant.

Table 2
F-ratio test values calculated for each pair of isotherm models, calculated from the sum of the squares of the fit residuals between the theoretical adsorption data and the experimental adsorption data of phenol

F_{t_1/t_2}	Isotherm models t1							
	LF (3)	T (3)	L–L (4)	L–LF (5)	L–T (5)	LF–LF (6)	T–T (6)	L–L–L (6)
Isotherm models t2								
LF (3)	1	3.7	71.8	233.5	388.8	229.7	345.4	397.4
T (3)		1	19.4	63.3	105.4	62.3	93.6	107.7
L–L (4)			1	3.3	5.4	3.2	4.8	5.5
L–LF (5)				1	1.7	1.0	1.5	1.7
L–T (5)					1	0.6	0.9	1.0
LF–LF (6)						1	1.5	1.7
T–T (6)							1	1.2
L–L–L (6)								1

The number in parenthesis is the number of estimated parameters in the model.

between them will be helped by considering the affinity energy distribution. Fig. 3 shows the results of the direct calculation of the adsorption affinity distribution derived from the isotherm data. The figure shows a plot of the fraction of the total surface occupied by sites i as a function of the logarithm of the adsorption-desorption constant $b(\epsilon_i)$ of phenol. A total of 10^8 iterations was necessary to obtain these results. Strikingly, the AED is a trimodal distribution. The presence of the third, well-separated energy mode at high energy mirrors the fact that the linear range of the isotherm is reached only at *very* low concentrations (the highest energy sites are the first to be populated when concentration increases above 0). The frontal analysis data show that it is only for concentrations lower than $0.075\,g\,l^{-1}$ that the breakthrough curves display no longer a front shock (characteristic of the non-linear behavior of the isotherm and of a significant gradient of concentration velocities). Only below this concentration of $0.075\,g\,l^{-1}$ does a symmetrical diffuse front is recorded. This demonstrates the importance of acquiring isotherm data in a wide concentration range, from very low (below $0.075\,g\,l^{-1}$) to very high concentrations (up to $75\,g\,l^{-1}$) to scan all the possible adsorption energies. Thus, a dynamic range of 1000 was required in this work. This is rather typical of the problems encountered in the investigation of heterogeneous surfaces.

Table 3
Comparison between the best isotherm parameters accounting for by the adsorption of phenol on the monolithic column (tri-Langmuir model) derived from the AED calculations and the Marquardt fitting procedure

	AED	Fitting
$q_{S,1}$ ($g\,l^{-1}$)	237	253
b_1 ($L\,g^{-1}$)	0.0095	0.0084
$q_{S,2}$ ($g\,l^{-1}$)	110	121
b_2 ($L\,g^{-1}$)	0.134	0.140
$q_{S,3}$ ($g\,l^{-1}$)	28	20
b_3 ($L\,g^{-1}$)	0.402	0.497

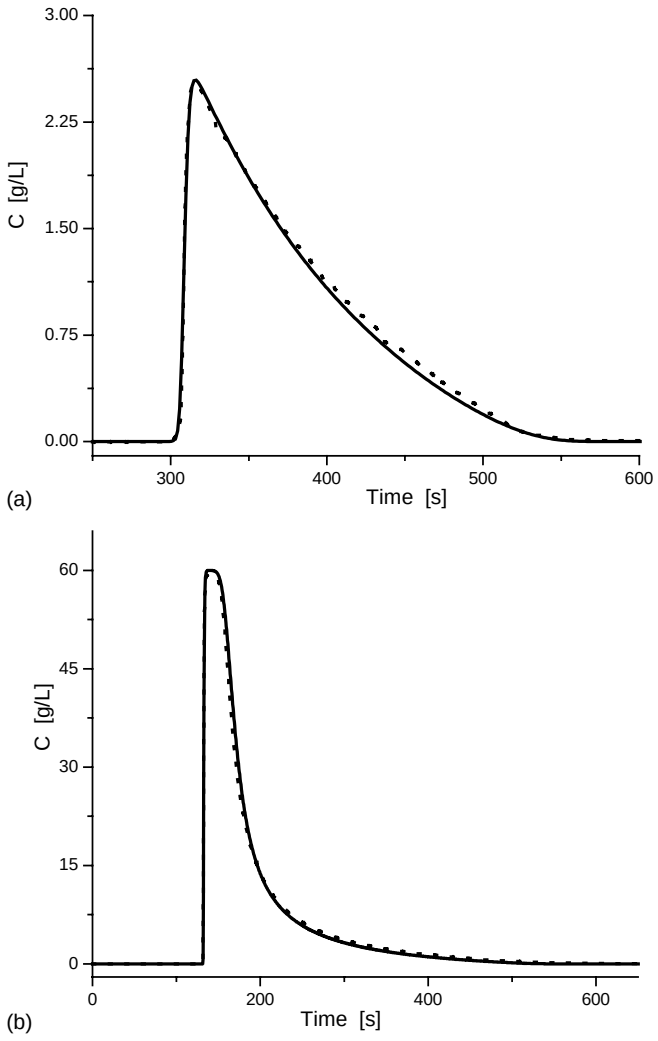

Fig. 4. Validation of the tri-Langmuir isotherm model for the adsorption of phenol on the Chromolith column. Comparison between the experimental (dotted line) and simulated (solid line) overloaded band profiles. (A) Low loading. (B) High loading. The simulation was performed by using the equilibrium-dispersive model assuming the tri-Langmuir isotherm model, an efficiency of 1000 plates and a rectangular injection (1 min at 5 and $60\,g\,l^{-1}$).

Accordingly, all the isotherm models (L–LF, L–T, LF–LF, T–T) that correspond to a bimodal AED are not consistent with our experimental adsorption data, despite the satisfactory fit obtained for these data. The only simple trimodal adsorption isotherm listed earlier is the tri-langmuir model (L–L–L). Table 3 compares the best parameters of the L–L–L isotherm model derived from the fit of the isotherm data to this model and those given by the AED calculations. They are in good agreement, confirming that the adsorption data of phenol on the C_{18}-Chromolith column can be satisfactorily accounted for only with an isotherm model corresponding to an AED with three distinct adsorption energies ($\epsilon_1 \leq \epsilon_2 \leq \epsilon_3$). The distances between these energy modes are equal to a few times *RT*, the thermal energy unit:

$$(\epsilon_2 - \epsilon_1) \simeq 2.7RT$$

$$(\epsilon_3 - \epsilon_2) \simeq 1.2RT$$

As demonstrated previously [12], the small adsorption energy differences between the three modes seem to imply that the interactions taking place on the corresponding sites are of a similar nature. On the surface of the C_{18}-bonded materials studied, it is likely that these sites can be assigned to specific locations on the adsorbent where the bonding densities differ significantly.

The validity of the tri-Langmuir isotherm model is supported by the excellent agreement between the experimental overloaded band profiles and those calculated using this isotherm, the equilibrium-dispersive model of chromatography, and an apparent column efficiency of 1000 plates. Fig. 4A and B show that this agreement is excellent both at low and at high column loadings. It is noteworthy that, without the information given by the AED calculations, it would have been impossible to choose between the five models remaining after the statistical analysis of the fit of the experimental data on these models (Table 2). The

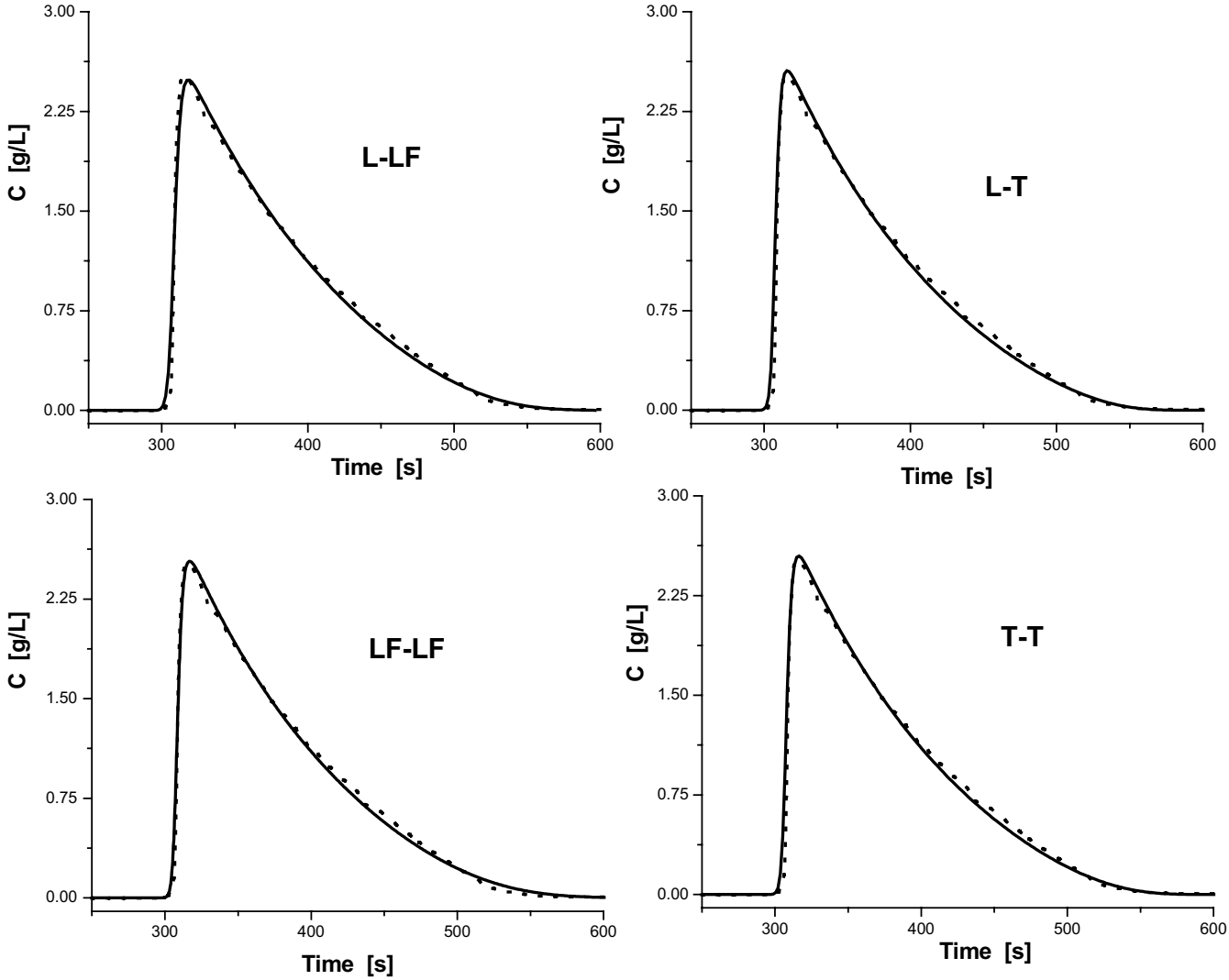

Fig. 5. Comparison between the experimental (dotted line) and simulated (solid line) overloaded band profiles of phenol on the Chromolith column for the four remaining isotherm models (L–LF, L–T, LF–LF and T–T). The simulation was performed by using the equilibrium-dispersive model, an efficiency of 1000 plates and a rectangular injection (1 min at 5 g l^{-1}).

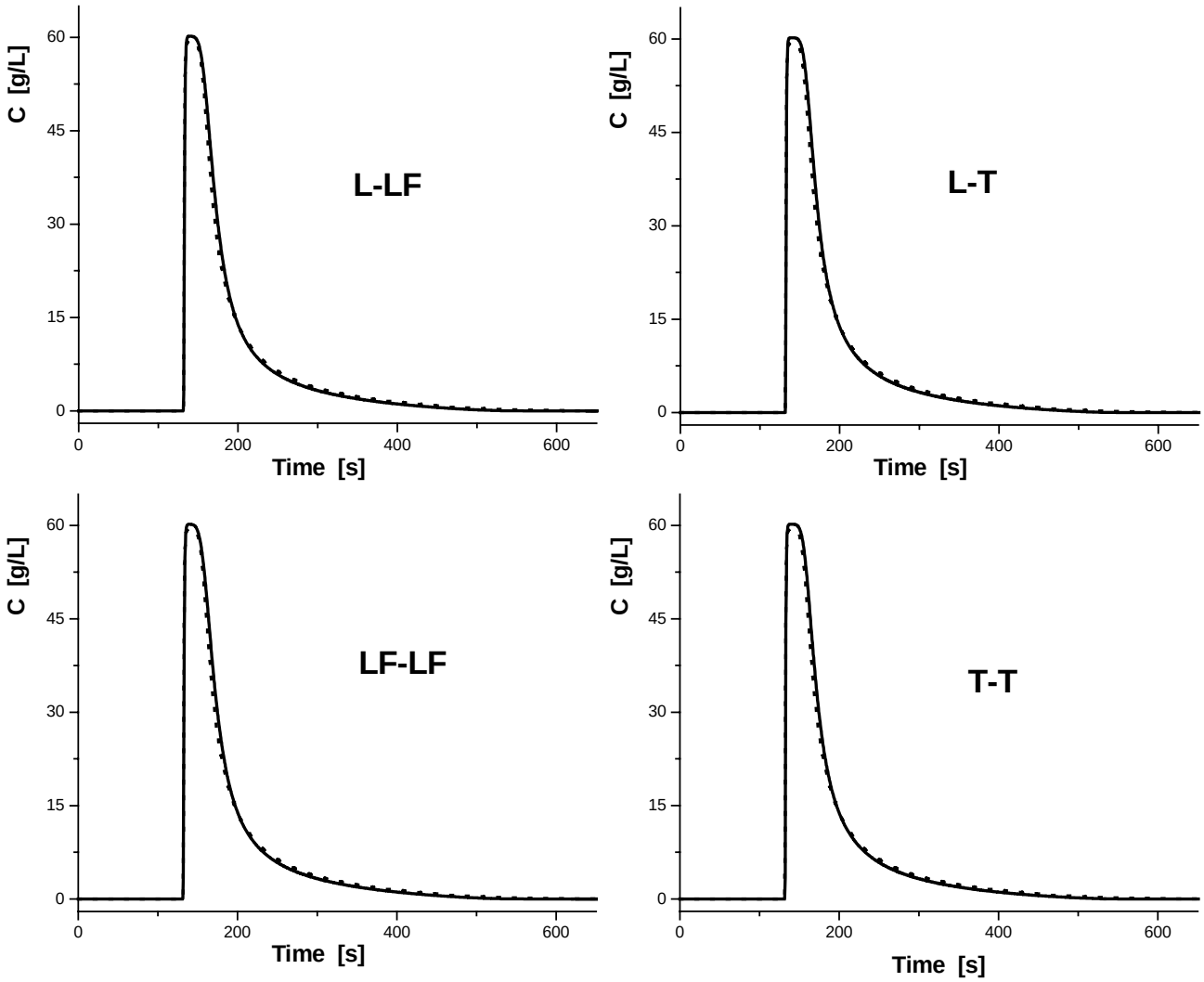

Fig. 6. Same as in Fig. 5 except the injected concentration = 60 g l^{-1}.

five-parameters L–T model might have been preferred to the six-parameters L–L–L model on the ground of having fewer parameters. However, Figs. 5 and 6 compare the experimental and the band profiles calculated using the four other isotherm models, L–LF, L–T, LF–LF and T–T. These figures exhibit an agreement as good as the one observed in Fig. 4A and B.

AED exhibiting three well-separated energy modes are exceptional so far in liquid chromatography. Most often, the surface heterogeneity is well accounted for by a bimodal energy distribution. For instance, under similar experimental conditions, using methanol/water solutions as the mobile phase, with a methanol concentration between 0 and 60%, the AED of phenol is bimodal on a packed C_{18}-Kromasil column [13,27,28]. It is well known that the bonded C_{18}-chains tend to collapse in a water-rich mobile phase, folding onto themselves (hydrophobic effect). This may contribute to enhance the adsorbent heterogeneity. A variety of local -C_{18}-structures may take place. These can be probed by small size solutes which are sensitive to small variations of the structure of the adsorbent "surface". In order to confirm the surface heterogeneity of the C_{18}-Chromolith stationary phase observed with phenol and to try and assign some physical sense to the three energy modes observed, we investigated the adsorption behavior of caffeine under the same experimental conditions.

4.2. Measurement of the adsorption isotherm of caffeine on the Chromolith performance column

Fig. 7A shows the adsorption data of caffeine on the C_{18}-Chromolith stationary phase measured by FA. The isotherm is clearly convex upward and the Scatchard plot convex downward (see Fig. 7B), so the best isotherm model must belong to the same sublibrary of isotherm as that of phenol. Following the same procedure and using the Fisher test selection eliminates the LF, T and L–L models (See Table 4). Among the other models, the one giving the highest F value is the bimodal T–T model. The five-parameters

Table 4
F-ratio test values calculated for each pair of isotherm models, calculated from the sum of the squares of the fit residuals between the theoretical adsorption data and the experimental adsorption data of caffeine

F_{t_1/t_2}	Isotherm models t1							
	LF (3)	T (3)	L–L (4)	L–LF (5)	L–T (5)	LF–LF (6)	T–T (6)	L–L–L (6)
Isotherm models t2								
LF (3)	1	12.6	29.5	348.8	482.6	359.2	564.1	458.9
T (3)		1	2.3	27.8	38.4	28.6	44.9	36.5
L–L (4)			1	11.8	16.3	12.2	19.1	15.5
L–LF (5)				1	1.4	1.0	1.6	1.3
L–T (5)					1	0.7	1.2	1.0
LF–LF (6)						1	1.6	1.3
T–T (6)							1	0.8
L–L–L (6)								1

The number in parenthesis is the number of estimated parameters in the model.

and the other six-parameters models give high F-factors too. To make a final decision between these models, we need to calculate the AED from the raw adsorption data of caffeine. The distribution obtained is quadrimodal (Fig. 8). Admittedly, the position and the area of the fourth, highest energy mode ($\ln b_4 = 2.02$, $q_{s,4} = 0.572$) if not questionable are inaccurate, particularly its area. The other three modes are well resolved and important. This result confirms the high degree of surface heterogeneity already observed for phenol.

Like for phenol, the energy modes are separated by a few times RT, also suggesting that the corresponding interactions are of a similar origin for all the modes:

$$(\epsilon_2 - \epsilon_1) \simeq 1.7RT$$
$$(\epsilon_3 - \epsilon_2) \simeq 1.3RT$$
$$(\epsilon_4 - \epsilon_3) \simeq 2.4RT$$

The isotherm data of caffeine were then fitted to a quadri-Langmuir isotherm model, having a total of eight parameters. In this case, the nonlinear least-squares regression program does not converge toward a single minimum because the number of model parameters is too large. In order to achieve convergence, we fixed the saturation capacity of the first Langmuir term, $q_{s,1} = 219.03$, at the very value of $q_{s,1}$ found with the AED calculations. Table 5 compares the seven other coefficients (b_1; $q_{s,2}$; b_2; $q_{s,3}$; b_3; $q_{s,4}$; b_4)

Table 5
Comparison between the best isotherm parameters accounting for by the adsorption of caffeine on the monolithic column (quadri-Langmuir model, $q_{S,1} = 219.0\,\mathrm{g\,l^{-1}}$) derived from the AED calculations and the Marquardt fitting procedure

	AED	Fitting
b_1 ($\mathrm{L\,g^{-1}}$)	0.0307	0.0314
$q_{S,2}$ ($\mathrm{g\,l^{-1}}$)	38.6	35.2
b_2 ($\mathrm{L\,g^{-1}}$)	0.176	0.181
$q_{S,3}$ ($\mathrm{g\,l^{-1}}$)	25.8	26.3
b_3 ($\mathrm{L\,g^{-1}}$)	0.654	0.644
$q_{S,4}$ ($\mathrm{g\,l^{-1}}$)	0.57	0.66
b_4 ($\mathrm{L\,g^{-1}}$)	7.52	6.84

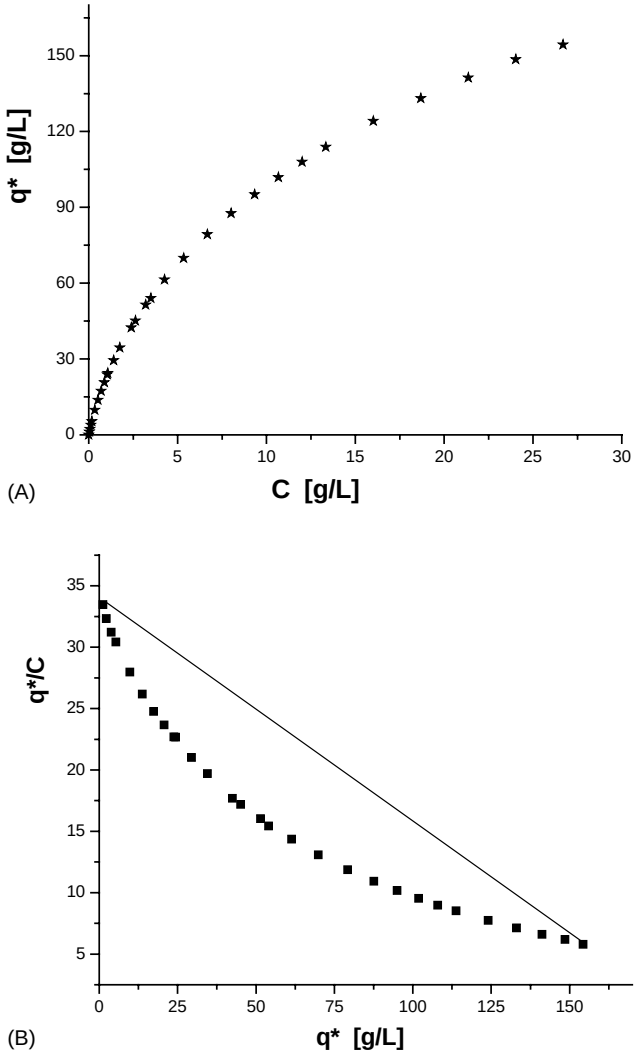

Fig. 7. Experimental isotherm (A) and Scatchard plot (B) of caffeine on the Chromolith column #30. Mobile phase methanol/water, 15/85 (v/v). $T = 296\,\mathrm{K}$.

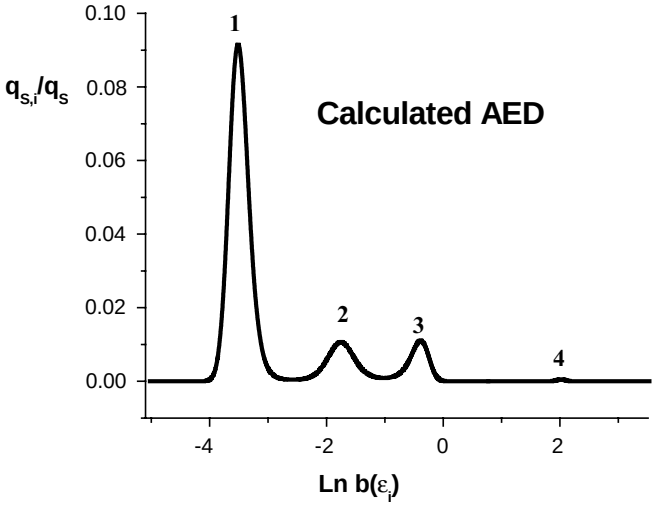

Fig. 8. Affinity energy distribution (AED) of caffeine on the Chromolith column, calculated by using the expectation–maximization method (EM). 10^8 iterations required. The AED is plotted as the fraction of the adsorbent surface as a function of the logarithm of the adsorption constant.

afforded by the linear regression of the isotherm data to the seven-parameters quadri-Langmuir equation and those derived by the EM method. All are in very good agreement, within less than a few percents, except for the saturation capacity and the equilibrium constant of the highest energy band 4, which differ by 15 and 9%, respectively.

The overloaded band profiles calculated with the best quadri-Langmuir isotherm are in excellent agreement with the experimental ones (Fig. 9A and B). However, the profiles calculated using the five simpler models (i.e., L–L–L, T–T, LF–LF, L–T, L–LF) are also in most satisfactory agreement with the experimental band profiles (Figs. 10 and 11). This confirms the importance of considering the results of the AED calculations in selecting the most appropriate isotherm model. The use of the AED introduces another physical criterion that completes the requirements for the choice of the best isotherm model, the other one being their ability correctly to predict overloaded band profiles. In a previous work, consideration of the AED was used to prefer a bimodal bi-Langmuir model to a unimodal Toth model in order to account for the adsorption of phenol and caffeine on a C_{18}-Kromasil column [11]. Despite the different mobile phase composition (the mobile phase used in this work contains more water), it is surprising to observe such a large difference between the adsorption heterogeneity of a packed and a monolithic columns that have the same average C_{18}-chains density ($\simeq 3.6\,\mu mol\,m^{-2}$) and comparable specific surface areas. The AED of caffeine is clearly bimodal on the Kromasil column [12] while it is at least trimodal with the monolithic column used here. Questions arise to know whether or not the silica structure may affect the homogeneity of the C_{18}-chain coverage after the bonding process. Genh and Loh [29] attributed, among different sources, the heterogeneity of surface energies to “the

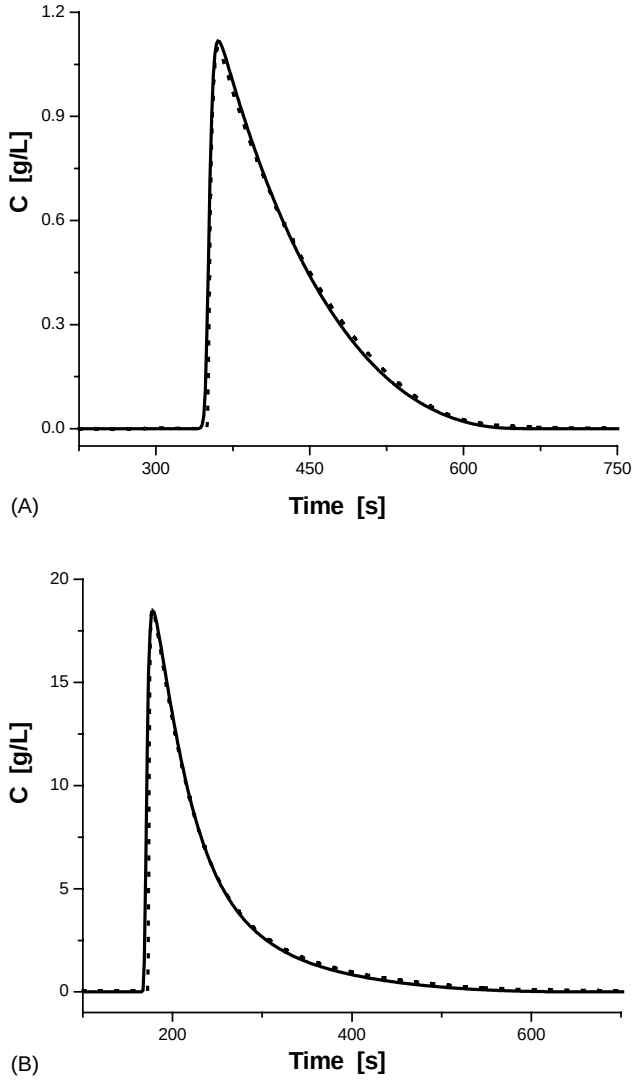

Fig. 9. Validation of the quadri-Langmuir isotherm model for the adsorption of caffeine on the Chromolith column. Comparison between the experimental (dotted line) and simulated (solid line) overloaded band profiles. (A) Low loading. (B) High loading. The simulation was performed by using the equilibrium-dispersive model assuming the tri-Langmuir isotherm model, an efficiency of 700 plates and a rectangular injection (1 min at 1.75 and $21.6\,g\,l^{-1}$).

presence of various pores of different sizes and shapes” in perfusive porous beds based on polymeric material.

4.3. Comparison of the adsorption isotherms of caffeine and phenol

The first three adsorption constants, b_i, are systematically larger for caffeine than for phenol, by factors of 3.69, 1.26 and 1.31 for the first, second and third constants, respectively. By contrast, the saturation capacities of the three modes of caffeine (reported in $mol\,l^{-1}$) are about twice smaller on site 1; seven times smaller on site 2; and 1.5 times smaller on site 3 than those of the corresponding modes of phenol. The first type of sites has the largest saturation

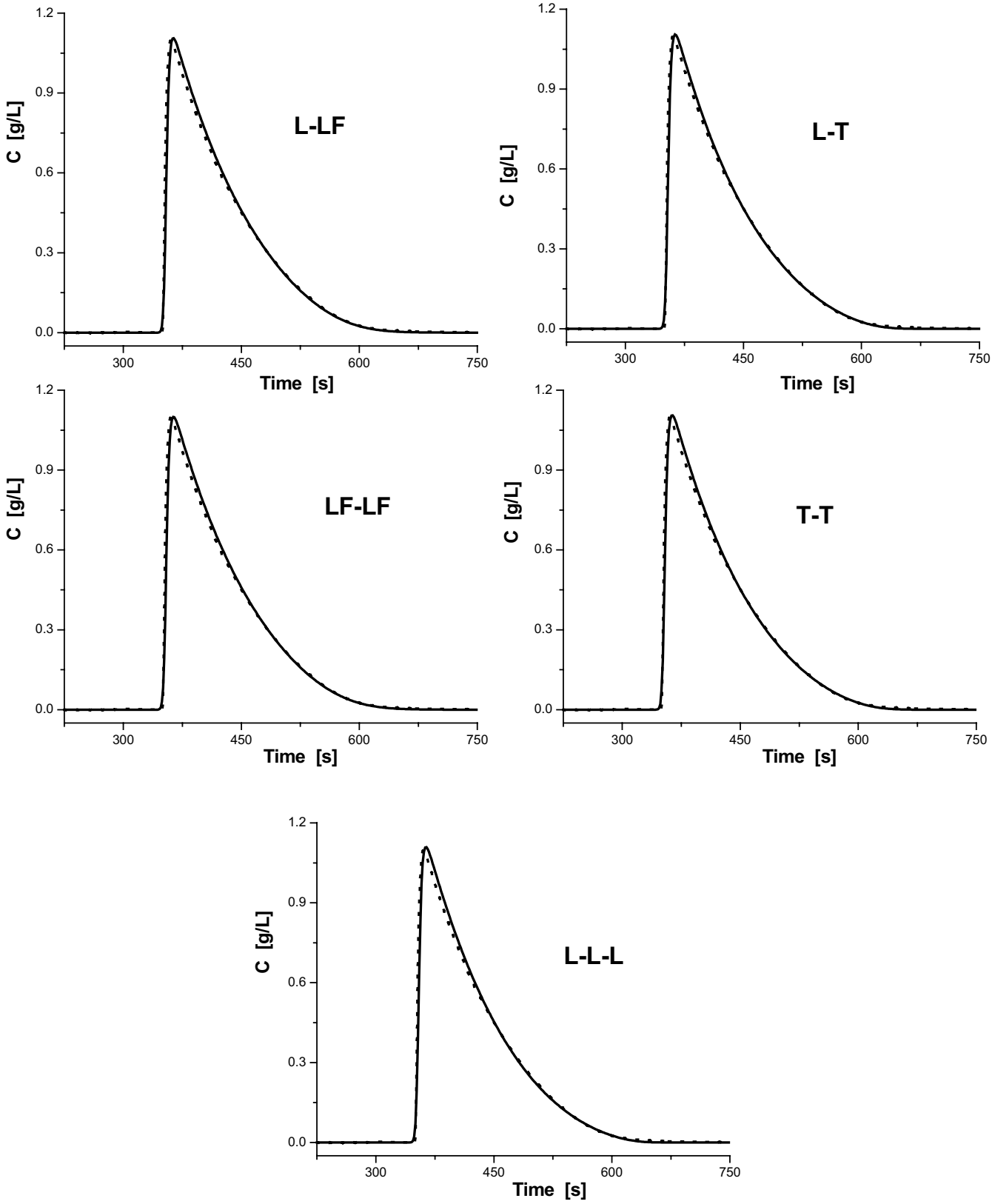

Fig. 10. Comparison between the experimental (dotted line) and simulated (solid line) overloaded band profiles of caffeine on the Chromolith column for the four remaining isotherm models (L–LF, L–T, LF–LF, T–T and T–T–T). The simulation was performed by using the equilibrium-dispersive model, an efficiency of 700 plates and a rectangular injection (1 min at 1.75 g l^{-1}).

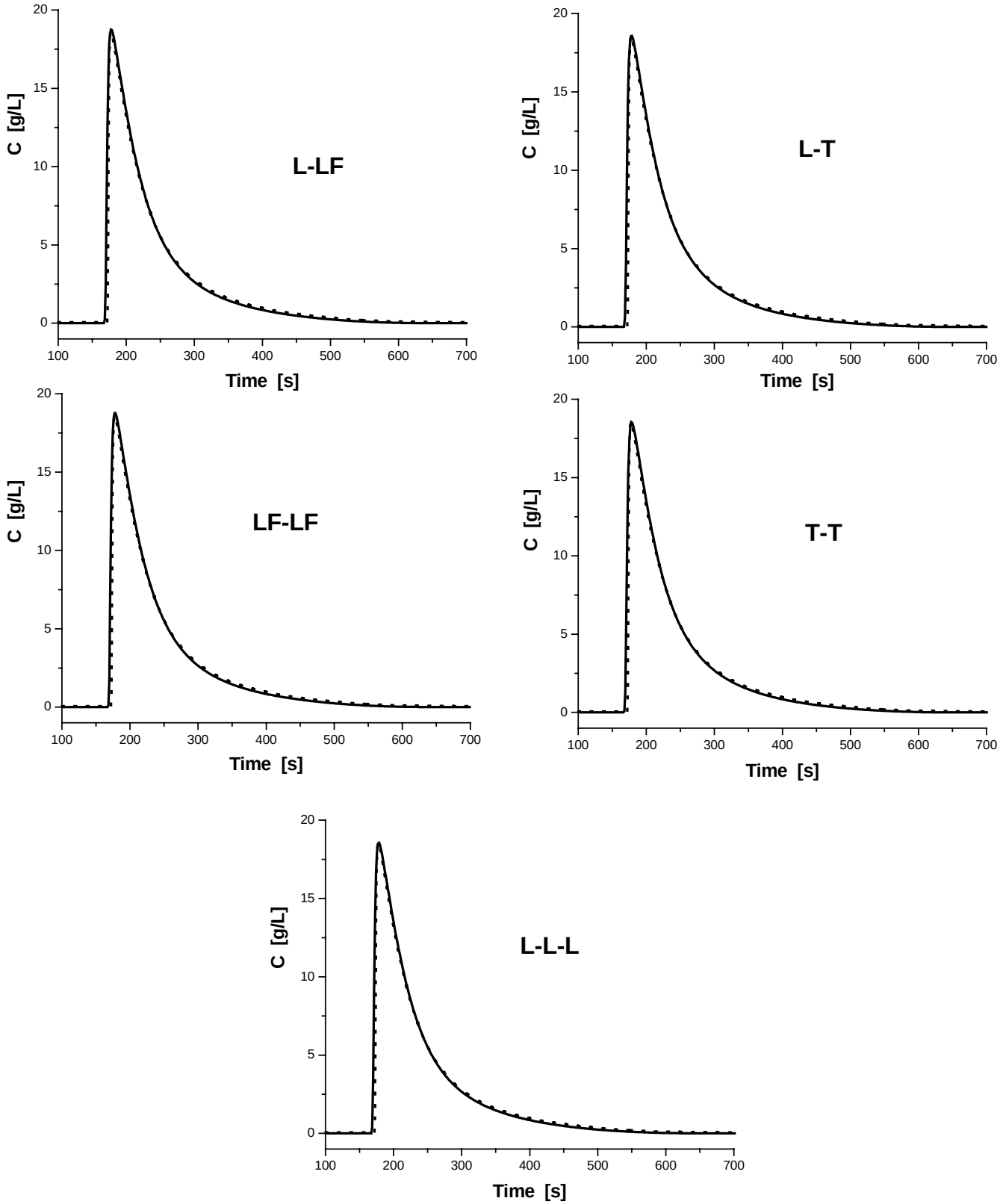

Fig. 11. Same as in Fig. 10 except the injected concentration = 21.6 $g\,l^{-1}$.

capacity (2.7 and 1.1 mol l^{-1} for phenol and caffeine, respectively) and the smallest binding constants (0.0083 and 0.0307 L g^{-1}, respectively). These observations combined with the larger molecular weight of caffeine (194 Da versus 94 Da for phenol) and its larger surface area of contact with the C_{18}-chains layer suggest that only adsorption takes place on these sites.

On the second type of sites, a large difference in the saturation capacities of the two compounds is observed (1.3 and 0.2 mol l^{-1} for phenol and caffeine, respectively) and the adsorption energies are 6 and 17 times larger than those observed on the first type of sites. This second type of sites is easily accessible to small size molecules like phenol. Conversely, the probability that a twice larger molecule like caffeine can access these sites is weak. This description of C_{18}-bonded silica adsorbents made of two sorts of sites is in agreement with what has been reported before on various packed columns [12]. It explains why, despite a larger molecular weight and a lower solubility in the mobile phase, caffeine is less retained than phenol on these columns. Caffeine is strongly excluded and a partition mechanism probably takes place on the second types of sites, the alkyl ligands being unable to fold sufficiently to accommodate the larger molecule.

Similar experimental observations were made on a series of five packed columns, using a 70/30 methanol/water solution as the mobile phase [12]. In this case, two adsorption energy modes only were observed. The first one is associated with an adsorption mechanism (site 1), the other with a partition mechanism. The saturation capacity of caffeine was lower than that of phenol on this second site by about the same factor, which was explained by steric hindrance. The main difference with the monolithic column is the existence in the latter case of a third type of adsorption sites that has a small but still significant (0.21 and 0.13 mol l^{-1} for phenol and caffeine, respectively) saturation capacity, hence is nearly as accessible to the two solutes. This might be explained by some nonselective adsorption sites present on the monolithic column but not on a packed column. The third energy mode found for the adsorption of both compounds and the possible fourth energy mode found for the adsorption of caffeine are likely to be specific of the new monolithic supports.

5. Conclusion

The adsorption data of phenol and caffeine acquired on a new C_{18}-Chromolith column (Merck) using an aqueous solution of methanol (85/15, v/v) as the mobile phase and the affinity energy distributions derived from these isotherms showed that the surface is heterogeneous, with a trimodal and a quadrimodal distributions for phenol and caffeine, respectively. The energy differences between the different modes are relatively small, suggesting that the lowest energy mode could correspond to adsorption at the interface between the solution and the hydrocarbon layer while the second and higher modes would be related to the dissolution of these adsorbed molecules inside the hydrocarbon layer. This work underlines the importance of performing accurate measurements of equilibrium isotherm data, of acquiring a sufficiently large number of data points, and of making sure that these data points are spread across a wide range of concentrations, extending from the quasi-linear part of the isotherm to the maximum solubility of the compound investigated. The lowest two energy modes are compatible with the similar modes observed on classical packed columns. By contrast, the highest (for phenol) or highest two (for caffeine) energy modes found in the AED seem to be specific of the new monolithic adsorbent. They might be related to details of its porous structure. The rather low energy of these modes suggest that they are not due to underivatized area of the silica adsorbent surface. In a recent submitted paper, we have investigated the adsorption of the same compounds on other C_{18}-bonded silicas having different polarity and structure. Results reinforce the idea, still provoking and undesirable by most concerned scientists, that the high-energy sites detected in this study are related to dispersion forces within the structure of C_{18}-bonded layer rather than the existence of strong interaction involving “active sites” (like free silanols) [30].

6. Nomenclature

b_0	preexponential factor of the binding constant
$b(\epsilon)$	binding constant associated to the adsorption energy ϵ (L g^{-1})
b_{min}	low boundary of the binding constant range use for the affinity energy distribution (L g^{-1})
b_{max}	high boundary of the binding constant range use for the affinity energy distribution (L g^{-1})
C	concentration of the solute in the mobile phase (g l^{-1})
C_1	first and lowest concentration of the solute in the mobile phase applied during frontal analysis measurement (g l^{-1})
C_j	jth concentration of the solute in the mobile phase applied during frontal analysis measurement (g l^{-1})
C_M	Mth and highest concentration of the solute in the mobile phase applied during frontal analysis measurement (g l^{-1})
D_a	apparent axial dispersion coefficient (cm^2/s)
$F(\epsilon)$	affinity energy distribution function (mol s^2 l^{-1})
$F^0(\epsilon_i)$	uniform distribution of the affinity energy distribution function corresponding to the initial guess of the AED calculation
$F^k(\epsilon_i)$	affinity energy distribution function estimated at the kth iteration during the AED calculation (mol s^2 l^{-1})

$F_{\mathrm{calc},t}$	Fisher number calculated for a given model $\mathcal{M}_t$
$F_{N-l_1,N-l_2,\alpha}$	element of the Student table (row $N-l_1$, line $N-l_2$, risk α)
F_{t_1,t_2}	F-test ratio calculated between two models, $\mathcal{M}_{t_1}$ and $\mathcal{M}_{t_2}$
l	number of adjusted parameters in a given isotherm model
L	length of the chromatographic column (m)
M	number of adsorption data or concentration in the mobile phase applied during frontal analysis measurement
N	number of grid points in the energy space
N_a	column efficiency
q^*	equilibrium solute concentration adsorbed on the stationary phase ($\mathrm{g\,l^{-1}}$)
q^k_{cal}	equilibrium solute concentration adsorbed on the stationary phase calculated at the kth iteration of the AED calculation ($\mathrm{g\,l^{-1}}$)
$q(C_M)$	equilibrium solute concentration adsorbed on the stationary phase for the highest concentration in the mobile phase performed during frontal analysis ($\mathrm{g\,l^{-1}}$)
$q_{\mathrm{exp},j}$	equilibrium solute concentration adsorbed on the stationary phase measured by frontal analysis for the concentration C_j in the mobile phase ($\mathrm{g\,l^{-1}}$)
$\overline{q_{\mathrm{exp}}}$	mean value of the adsorbed data, $q_{\mathrm{exp},j}$ ($\mathrm{g\,l^{-1}}$)
q_s	total saturation capacity ($\mathrm{g\,l^{-1}}$)
$q_{s,i}$	saturation capacity of sites i ($\mathrm{g\,l^{-1}}$)
$q_{t,j}$	estimate of the stationary phase concentration of the adsorbate by a given model, $\mathcal{M}_t$ ($\mathrm{g\,l^{-1}}$)
R	ideal molar gas constant ($\mathrm{kJ\,mol^{-1}\,K^{-1}}$)
t	time (s)
T	temperature (K)
u	interstitial linear velocity ($\mathrm{m\,s^{-1}}$)
V_0	hold-up colum volume (l)
V_a	stationary phase volume (l)
V_eq	elution volume of the equivalent area in frontal analysis (l)
z	longitudinal distance along the column (m)

Greek letters

ϵ	continuous adsorption energy variable ($\mathrm{kJ\,mol^{-1}}$)
ϵ_{max}	highest discretized adsorption energy ($\mathrm{kJ\,mol^{-1}}$)
ϵ_{min}	lowest discretized adsorption energy ($\mathrm{kJ\,mol^{-1}}$)
ϵ_i	discretized adsorption energy variable ($\mathrm{kJ\,mol^{-1}}$)
$\Delta\epsilon$	adsorption energy step ($\mathrm{kJ\,mol^{-1}}$)

Acknowledgements

This work was supported in part by grant CHE-0244696 of the National Science Foundation and by the cooperative agreement between the University of Tennessee and the Oak Ridge National Laboratory. We thank Karin Sinz and Karin Cabrera (Merck, Darmstadt, Germany) for the generous gift of the columns used in this work and for fruitful discussions.

References

[1] G. Guiochon, S.G. Shirazi, A.M. Katti, Fundamentals of Preparative and Nonlinear Chromatography, Academic Press, Boston, MA, 1994.
[2] G. Guiochon, J. Chromatogr. A 965 (2002) 129.
[3] B. Lin, G. Guiochon, Modeling for Preparative Chromatography, Elsevier, Amsterdam, The Netherlands, 2003.
[4] D.M. Ruthven, Principle of Adsorption and Adsorption Processes, Wiley, New York, NY, 1984.
[5] G. Schay, G. Szekely, Acta Chem. Hung. 5 (1954) 167.
[6] D.H. James, C.S.G. Phillips, J. Chem. Soc. (1954) 1066.
[7] E. Glueckauf, Trans. Faraday Soc. 51 (1955) 1540.
[8] E. Cremer, G.H. Huber, Angew. Chem. 73 (1961) 461.
[9] F.G. Helfferich, D.L. Peterson, J. Chem. Educ. 41 (1964) 410.
[10] C. Blümel, P. Hugo, A. Seidel-Morgenstern, J. Chromatogr. A 827 (1998) 175.
[11] F. Gritti, G. Götmar, B. Stanley, G. Guiochon, J. Chromatogr. A 988 (2003) 185.
[12] F. Gritti, G. Guiochon, Anal. Chem. 75 (2003) 5726.
[13] F. Gritti, G. Guiochon, J. Chromatogr. A 995 (2003) 37.
[14] G. Zhong, P. Sajonz, G. Guiochon, Ind. Eng. Chem. (Res.) 36 (1997) 506.
[15] M. Jaroniec, R. Madey, Physical Adsorption on Heterogeneous Solids, Elsevier, Amsterdam, The Netherlands, 1988.
[16] R.J. Umpleby II, S.C. Baxter, Y. Chen, R.N. Shah, K.D. Shimizu, Anal. Chem. 73 (2001) 4584.
[17] J. Toth, Adsorption, Marcel Dekker, New York, NY, 2002.
[18] B.J. Stanley, S.E. Bialkowski, D.B. Marshall, Anal. Chem. 659 (1994) 27.
[19] A. Cavazzini, F. Gritti, K. Mihlbachler, G. Guiochon, Workshop Presented at the 16th International Symposium on Preparative/Process Chromatography, San Francisco, CA, 29 June–2 July 2003.
[20] D.W. Marquardt, J. Soc. Appl. Math. 11 (1963) 431.
[21] M. Suzuki, Adsorption Engineering, Elsevier, Amsterdam, The Netherlands, 1990.
[22] K. Kaczmarski, M. Mazzotti, G. Storti, M. Morbidelli, Comput. Chem. Eng. 21 (1997) 641.
[23] K. Kaczmarski, Comput. Chem. Eng. 20 (1996) 49.
[24] K. Kaczmarski, D. Antos, J. Chromatogr. A 862 (1999) 1.
[25] P.N. Brown, A.C. Hindmarsh, G.D. Byrne, Procedure available from http://www.netlib.org.
[26] P.W. Danckwerts, Chem. Eng. Sci. 2 (1953) 1.
[27] F. Gritti, G. Guiochon, J. Chromatogr. A 1010 (2003) 153.
[28] F. Gritti, A. Felinger, G. Guiochon, J. Chromatogr. A 1017 (2003) 45.
[29] A. Geng, K.C. Loh, J. Colloid Interface Sci. 239 (2001) 447.
[30] F. Gritti, G. Guiochon, J. Chromatogr. A 1028 (2004) 75.